Self-Limiting Chemical Vapor Deposition Growth of Monolayer Graphene from Ethanol

Pei Zhao,[a] *Akihito Kumamoto,*[b] *Sungjin Kim,*[a] *Xiao Chen,*[a] *Bo Hou,*[a] *Shohei Chiashi,*[a] *Erik Einarsson,*[a,c] *Yuichi Ikuhara,*[b] *Shigeo Maruyama*,*[a]

[a] Department of Mechanical Engineering, The University of Tokyo,

Hongo 7-3-1, Bunkyo-ku, Tokyo 113-8656, Japan

[b] Institute of Engineering Innovation, The University of Tokyo

Yayoi 2-11-16, Bunkyo-ku, Tokyo 113-8656, Japan

[c] Global Center of Excellence for Mechanical Systems Innovation, The University of Tokyo,

Hongo 7-3-1, Bunkyo-ku, Tokyo 113-8656, Japan

*Author email: maruyama@photon.t.u-tokyo.ac.jp

TEL: +81-3-5841-6421 FAX: +81-3-5800-6983

Abstract

Using low-pressure chemical vapor deposition (LPCVD), we for the first time realize the self-limiting growth behavior of monolayer graphene on commercially available electroplated copper foils from a carbon precursor other than methane, and systematically investigate the growth of graphene from ethanol and compare its self-limiting behavior over copper facets with different identities. Results show that the growth of graphene from ethanol in the LPCVD process is a substrate-mediated process, in which the domains of graphene are determined by the lattice axes on the copper facets. Moreover, during the evolution of the domains, low-index copper facets of Cu(111) and Cu(100) play a critical role in the following self-limiting process of a continuous graphene sheet, whereas the Cu(110) and high-index facets favor nucleation and formation of secondary layers. In addition, a high degree of similarity exists between graphene grown from ethanol and methane, showing that when the carbon flux is sufficiently low, the self-limiting growth of graphene on copper surfaces using LPCVD is independent of the precursor structure of ethanol and methane.

KEYWORDS: graphene, ethanol, self-limiting, chemical vapor deposition, copper facet

1. Introduction

Its two-dimensional nature has made graphene—a one-atom-thick crystal with sp^2-carbon honeycomb structure—one of the most attractive materials for next-generation technologies in many fields due to its superior properties in mechanical strength and flexibility,[1] electrical carrier mobility,[2,3] thermal conductivity,[4,5] and so on. Having evolved from mechanical microcleavage,[6] reduction of graphene oxide,[7] epitaxial growth on silicon carbide,[8] to chemical vapor deposition (CVD) of hydrocarbon precursors on transition metals,[9-13] economic approaches to the production of graphene with large-scale and high-quality are always a key requirement for exploring graphene's numerous potential applications. As the most promising route to obtain graphene films up to wafer scale,[14,15] nickel and copper are the two most commonly used metal substrates. Due to the high solubility of carbon species in nickel (~0.9 atom% at 900 ºC),[16] the precipitation process of dissolved carbon determines that the graphene films grown on nickel surfaces always have small domain sizes and various layer numbers,[11] which to a large extent limits the usability. On the other hand, when copper is used as the catalytic substrate, the low solubility of carbon in copper (<0.001 atom% at 1000 ºC) restricts the growth of graphene to the metal surface.[12,17] The uniformity and high quality of the resultant graphene, as well as the easy operability of CVD, has made copper the most preferable substrate for growth of graphene in large-scale.

Moreover, because the polycrystalline structure of graphene considerably worsens its many exceptional properties,[18] one of the most critical tasks is the synthesis of high-quality single-crystal graphene films as large as wafer scale.[19] This requires a deep understanding of the growth

mechanism of graphene from different carbon precursors. Nowadays most CVD synthesis of graphene is conducted using methane, but low-pressure (LP) and atmospheric-pressure (AP) conditions exhibit different results and growth mechanisms. In the LPCVD case, graphene growth on copper is a surface-limited diffusion process of carbon species, during which the graphene domains have symmetric patterns with different lobes, such as six-lobed snowflake-like structures[20,21] and four-lobed star-like structures,[22] but sometimes with irregular shapes.[23] These patterns are expected to be associated with the underlying copper surface morphology,[24] such as roughness and crystal facet orientation. Self-limiting growth of graphene can be obtained using LPCVD, which terminates with monolayer films and very few areas covered by secondary nucleation. However, more detailed investigation on this self-limiting behavior influenced by the underlying copper morphology remains unclear. On the other hand, in the APCVD process, high flow rate and partial pressure of hydrogen are required, and to keep a fixed flow-rate ratio of hydrogen to methane, the partial pressure of methane has to be correspondingly increased.[17] The growth in APCVD is not self-limiting, and likely to be a surface-adsorption process in which extended growth time results in an increase in the graphene layer number.[17] This is due to the high levels of carbon supersaturation on the copper surface due to excess carbon supply.[25] Moreover, the graphene domains usually exhibit a hexagonal shape,[19,25,26] suggesting a growth mechanism that is determined by the graphene structure rather than the underlying copper substrates. This is also consistent with a previous scanning tunneling microscopy (STM) study on the continuity of graphene on polycrystalline copper using high-pressure CVD,[27] which shows that the underlying copper morphology and atomic arrangement do not affect the resulting graphene structure.

Here we report LPCVD growth of graphene on copper substrate using ethanol, and for the first time show that the self-limiting growth behavior of graphene is not exclusive to methane. We systematically investigate the continuity of graphene grown over copper facets with different indices, and reveal during the evolution of the graphene domains, that low-index copper facets of Cu(111) and Cu(100) play a critical role in the following self-limiting process of a continuous graphene sheet. Conversely, nucleation and formation of secondary layers is found to preferentially occur on Cu(110) and high-index facets. In addition, we find a high degree of similarity between graphene from ethanol and methane, suggesting that when the carbon flux is sufficiently low, self-limiting growth of graphene on copper surfaces using LPCVD is independent of the precursor structure of ethanol and methane.

2. Experimental Section

Synthesis: The ACCVD process was used for self-limiting growth of monolayer graphene.[28] Commercially available copper foils were first cleaned by diluted HCl to remove the protective layer on the surface, then immersed in acetone and 2-propanol for 15 min, respectively. The copper foil was then folded into an enclosure with the remaining three sides carefully crimped, as reported by Li et al.[20] The copper foil enclosure was then loaded into a hot-wall CVD quartz chamber (26 mm, i.d.), and heated to 1000 ºC under a 250 sccm flow of 3% H_2 in Ar at 230–260 Pa for 40 min. The enclosure was further annealed at 1000 ºC for 20 min to smooth the metal surface and remove any oxides. 10 sccm ethanol vapor diluted by 300 sccm flow of 3% H_2 in Ar was then introduced for different growth periods. The total pressure in the CVD chamber was kept at 300 Pa, with an ethanol partial pressure of ~10 Pa. After growth, the chamber was slowly cooled to ~700 ºC at a rate of 10–20 ºC·min^{-1}, during which the ethanol and Ar/H_2 flow was

maintained. Finally, the ethanol supply was stopped and the chamber was rapidly cooled to room temperature (~25 ºC).

Transfer: The transfer of as-grown graphene to arbitrary substrates is similar to the process reported in Ref.[12]. After unfolding the copper foil enclosure, a layer of 4 wt.% poly(methyl methacrylate) (PMMA, MW=950k, dissolved in anisole) was spin-coated onto the inside surface, and then baked at 150 ºC for 30–60 min. After baking, the outside surface was treated by oxygen plasma at 20 W for 2 min to remove any graphitic layers. A Cu etching process using 1 M $FeCl_3$ was then conducted to isolate the graphene/PMMA film for transferring to arbitrary substrates. Finally, the PMMA protection layer was removed by hot acetone bath (80 ºC), followed by annealing the sample at 360 ºC for 2–4 hr under an atmosphere of Ar/H_2.

Characterization: Characterization of as-grown and transferred graphene samples consisted of SEM (5 kV, S-4800, Hitachi Co., Ltd.), EBSD-SEM (20 kV, JSM-7000F, JEOL Co., Ltd.), TEM (100 kV, JEM-1400, JEOL Co., Ltd.), UV-vis-NIR spectroscopy (UV-3600, Shimadzu Co., Ltd.), AFM (SPI3800N, Seiko Instrument Inc.), and micro-Raman spectroscopy (Raman-11 system, Nanophoton Co., Ltd.).

3. Results and discussion

3.1. Self-limiting growth of monolayer graphene from ethanol

To realize self-limiting growth of graphene on Cu using methane, both the methane partial pressure and the total CVD pressure must be low, i.e., an LPCVD condition is required.[12] However, as for carbon precursors with more than one carbon atom, self-limiting growth is difficult to achieve even if the same LPCVD condition used for methane is employed,[29] but little

attention has been paid to the improvement of such growth from non-methane precursors and the corresponding growth mechanisms.[29-32]

We chose ethanol as the carbon precursor to study the LPCVD growth process of graphene, and constructed an ethanol-vapor-based CVD system as shown in Figure S1 in Supporting Information (SI). We previously reported that typical growth on copper foil using this system yields multi-layer graphene unless the growth time is less than 30 s.[33] This growth behavior is similar to that reported for graphene growth from methane at elevated pressure, but the growth time needed for methane is much longer. This is probably due to the lower dissociation bond-energy and higher reactivity of ethanol. We therefore suspected that if the ethanol flux were further reduced, an analogous behavior to graphene growth in LPCVD process using methane would become possible.

To test this hypothesis, a copper foil (10-μm-thick, product No. YB-10, Nippon Denkai, Ltd.) enclosure as reported by Li et al. was adopted.[20] This foil was produced by electroplating method, in which a layer of metal coating is formed on a rolling drum from the electrolyte, as shown in Figure S2 in SI. The key purpose of using an enclosure is to reduce the carbon flux. However, different from Ref.[20] in which methane results in only isolated single-crystal graphene domains on the inside surface of the enclosure, ethanol yields a continuous and uniform graphene sheet. Figure 1a shows a copper enclosure after graphene growth at typical growth conditions (1000 ºC, 10 sccm ethanol flow diluted by 300 sccm Ar/H_2, ethanol partial pressure of 10 Pa, growth time of 10 min, see Experimental Section). Figure 1b shows a scanning electron microscope (SEM) image obtained after the CVD process on the inside copper surface of the enclosure. The inside surface appears uniform and low contrast, and is later confirmed to be a graphene monolayer. Graphene domain boundaries are seen in Figure 1b, as well as wrinkles in

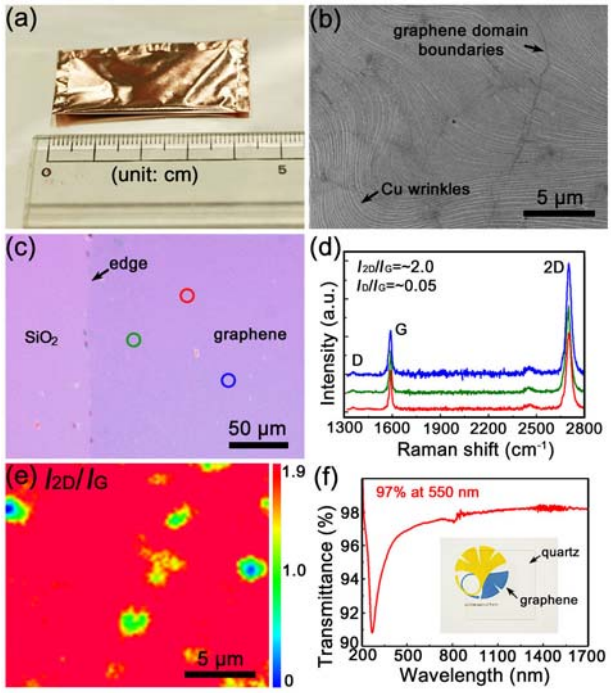

Figure 1. (a) Photograph of a crimped copper enclosure after the CVD process. (b) SEM image of graphene on the inside surface of a Cu enclosure after 10 min growth from ethanol. (c) Optical micrograph of a graphene film on a SiO_2 (300 nm)/Si substrate. (d) Raman spectra corresponding to the positions circled by red, green and blue in (c). (e) Raman scanning map showing I_{2D}/I_G of an ethanol-derived graphene film on a Si/SiO_2 substrate. (f) Transmittance of a graphene film on a quartz substrate. Inset photograph shows the transparency of the transferred graphene sample.

the foil. On the other hand, SEM images of the outside surface of the enclosure show regions of different contrast (Figure S3 in SI), consisting of slightly etched regions of graphene/graphite having different layer number. The pronounced difference between graphene grown on the inside and outside surfaces of the copper foil enclosure demonstrates that such an enclosure can effectively change the growth environment when using ethanol to be similar to LPCVD using

methane. An SEM image of this graphene film transferred onto a Si/SiO_2 substrate is shown in Figure S4 in SI, with small areas of bilayer graphene visible as dark dots.

The uniformity of as-grown monolayer graphene films can be evaluated optically by the slight color contrast that becomes apparent when the graphene layer is on top of a 300-nm-thick SiO_2 layer,[6] as shown in Figure 1c. Corresponding Raman spectra obtained from areas circled by red, blue and green are shown in Figure 1d. A typical Raman spectrum of graphene presents three dominant features: the G-band (~1582 cm^{-1}), D-band (~1350 cm^{-1}), and 2D-band (~2690 cm^{-1}). All Raman spectra obtained from the areas circled in Figure 1d are indicative of monolayer graphene, such as a 2D-band to G-band intensity ratio (I_{2D}/I_G) larger than 2, and a symmetric 2D-band with a full-width-at-half-maximum (FWHM) value of 32–35 cm^{-1}.[34] Moreover, the D-band to G-band intensity ratio (I_D/I_G) is only ~0.05, indicating very high quality of this ethanol-grown graphene. A scanning Raman contour map of I_{2D}/I_G shown in Figure 1e reveals the overall uniformity and quality of the graphene film within an area of 20 μm×17.5 μm (spatial resolution 300 nm), in which more than 99% of the obtained Raman spectra exhibit features of monolayer graphene (red and green parts), and less than 1% are bilayer graphene (blue part). The thickness of the graphene film was also evaluated using UV-vis-NIR spectroscopy, as shown in Figure 1f. After transferring to a quartz substrate, the graphene film exhibits a transmittance of 97% at 550 nm, close to the known value for monolayer graphene.[35]

We interrupted the CVD growth of graphene at various times to investigate its growth process. In Figures 2a-h we present a series of SEM images showing the stages of graphene grown on copper foil at a temperature of 1000 ºC. Because the secondary electron yield for copper is significantly higher than that for graphene, the graphene appears dark in these images. On occasion, oxidized contaminants—appearing as white dots—are present in the images.[26] Figures

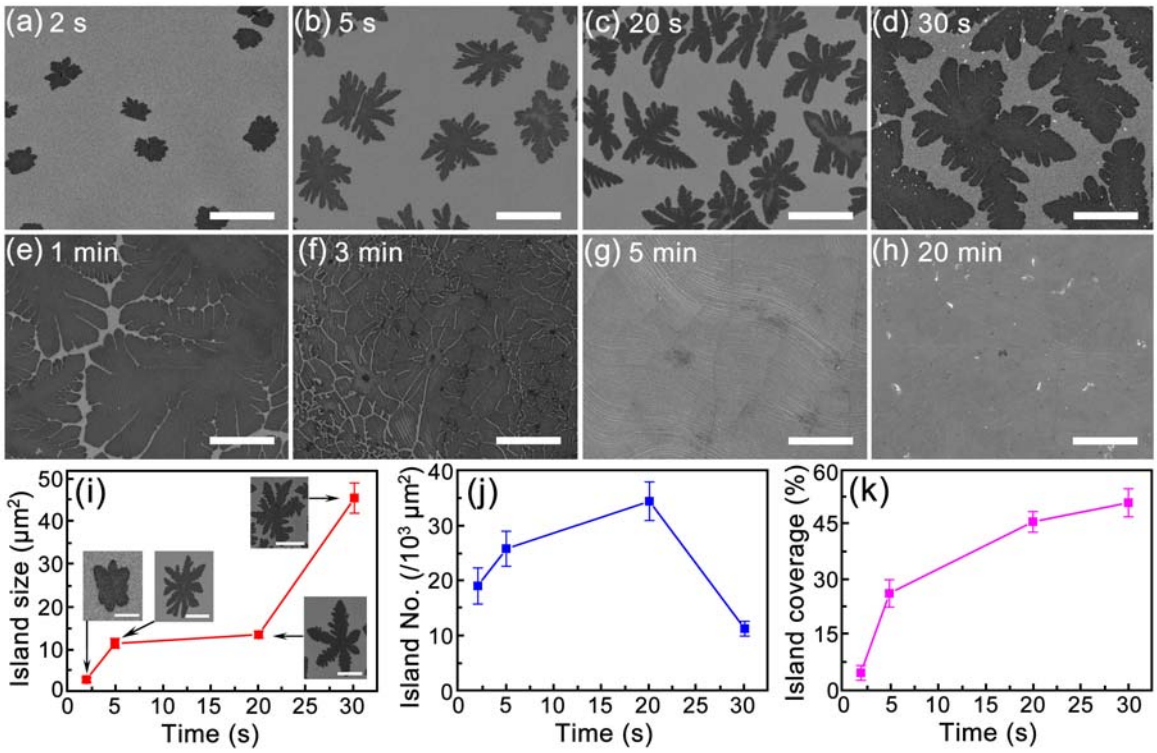

Figure 2. (a-h) SEM images of as-grown graphene on copper surface with different exposure times to ethanol. A self-limiting growth of monolayer graphene can be obtained after a growth period of 5 min. All scale bars in (a-h) are 5 μm. (i-k) The size, number and coverage of graphene islands as a function of growth time during the first 30 s of CVD. Scale bars in (i) for 2 s, 5 s, 20 s and 30 s are 2 μm, 3 μm, 3 μm and 10 μm, respectively.

2i-k show the size, number and surface coverage of graphene domains/islands as a function of growth time. Small graphene domains were found nucleated on the copper surface in less than 2 s. The size of the graphene domains significantly increased between 2 and 5 s, whereas the number of domains increased from 5 s to 20 s. Between 20 s and 30 s, the domains start to coalesce and form larger dendritic flakes and islands. The domains grown in the first 30 s exhibit a radially symmetric dendritic structure, most of which are six-lobed. Moreover, as shown in Figure 2k, the graphene surface coverage continues to increase with ethanol exposure time, but

the overbending shape of this curve indicates a decreasing growth rate with increased growth time. The coalescence behavior is more apparent when the growth time was increased to 60 s, but the coalesced graphene islands still appear dendritic rather than irregular. Growth of a continuous sheet of monolayer graphene was completed and terminated after 5 min of ethanol flow, and extended growth time resulted in no further growth.

Further investigations of the graphene domains are shown in Figure 3, in which the growth time was 20 s. After transfer to a Si/SiO_2 substrate, SEM observation (Figure 3a) shows that some of the graphene domains have a secondary nucleation at the center due to the higher carbon concentrations at these sites.[24] Figure 3b shows an atomic force microscope (AFM) image of a graphene domain transferred onto a Si/SiO_2 substrate. Selected-area electron diffraction (SAED) of these graphene domains using transmission electron microscopy (TEM) shows a single set of six-fold symmetric diffraction spots (Figure 3c), and the corresponding spot intensities along the red line clearly indicate a single crystal. We also performed scanning Raman mapping on these graphene domains. The spatial distributions of I_G, I_{2D}/I_G, and I_D for a single graphene domain are shown in Figures 3d-f. The Raman G-bands of the graphene domain exhibit uniform intensities except at the center (spot A), where intensities are significantly higher than in the other part of the domain. Typical I_{2D}/I_G values are larger than 2, and—again with the exception of spot A—the I_D associated with defects is negligible over the graphene domain.

We investigated the surface morphology of this electroplated copper foil by AFM and electron backscatter diffraction (EBSD), as shown in Figures 4a and b, respectively. Measurements were performed after annealing the Cu surface under Ar/H_2 at 1000 ºC, but prior to exposure to ethanol. AFM images show a large atomically flat region extending for hundreds of nanometers over the surface; the largest height variation is less than 2 nm and the root-mean-

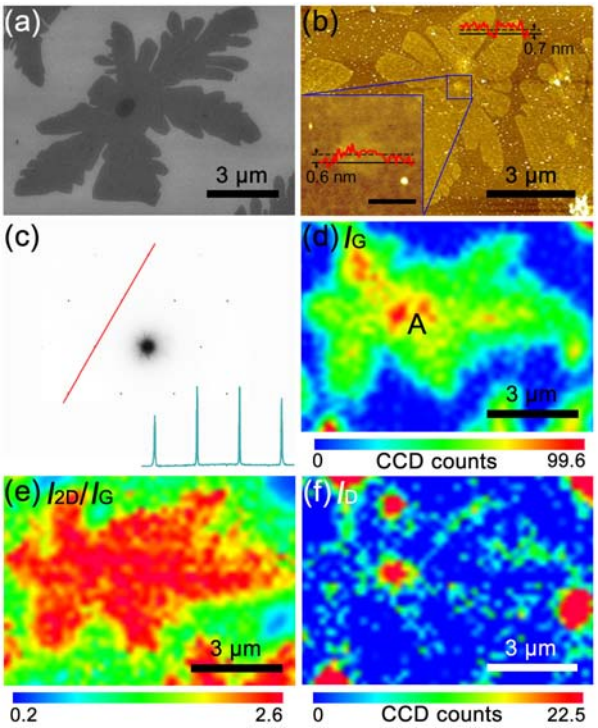

Figure 3. (a) SEM image of a graphene domain after transfer onto a SiO_2/Si substrate. (b) AFM image of a different graphene domain on a SiO_2/Si substrate. Inset shows the secondary nucleation area, and the scale bar is 300 nm. (c) SAED pattern of a graphene domain, which shows clear six-fold symmetry. Inset shows the spot intensities along the red line. (d-f) Raman scanning maps of a graphene domain showing I_G, I_{2D}/I_G and I_D values, respectively. Spot A shows the secondary nucleation of a graphene domain.

square (RMS) roughness is only 0.35 nm. The EBSD mosaic map in Figure 4b shows that the surface is composed of different facets, such as Cu(111), Cu(100) and Cu(101). The distribution of these facets is shown in Figure 4c, in which black, red and yellow dots indicate high, medium and low facet probabilities, respectively. The Cu(111) facet dominates the surface with a coverage of ~64.2%. This value was calculated from the ESBD map of the Cu(111) facet shown in Figure S5 in SI. The six-lobed dendritic structure of graphene domains suggests a mechanism

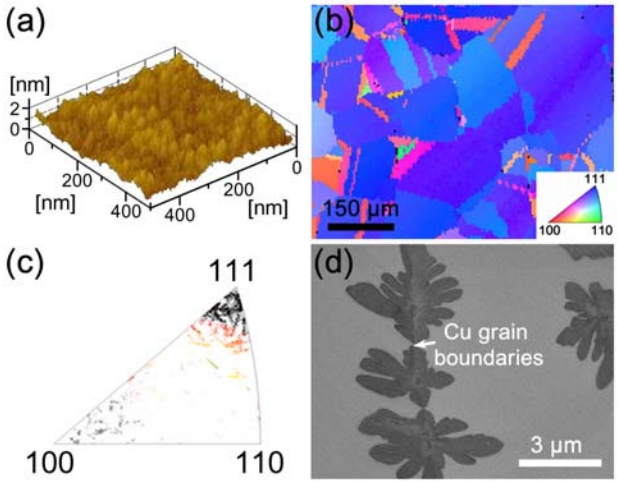

Figure 4. (a) AFM measurement and (b) EBSD mosaic map of the copper foil surface after annealing at 1000 ºC but prior to exposure to ethanol. (c) Coverage statistics of different copper facets shown in (b). Black, red and yellow dots indicate high, medium and low facet probabilities, respectively. (d) Growth of graphene domains at the grain boundary of a copper surface. I_G, I_{2D}/I_G and I_D values, respectively. Spot A shows the secondary nucleation of a graphene domain.

associated with the six-fold symmetry of the Cu(111) facet, however, these domains seem only weakly coupled with the underlying surface (Figure 4d) because they were frequently observed across the copper grain boundaries without modifying their dendritic symmetries.

When two graphene domains grow near each other, their regular dendritic symmetries are changed, as shown in Figures 5a and b. The domain edges exposed to more of the bare copper surface appear dendritic, whereas the extension of the edges close to the neighboring graphene domain is very limited. Moreover, after these two domains coalesce, this coalesced graphene island continues growing with dendritic fronts, as seen from the edges of the large graphene islands in Figure S6 in SI. Even when most of the adjacent domains have coalesced, the formed flakes and islands still exhibit flower-like and leaf-like structures.

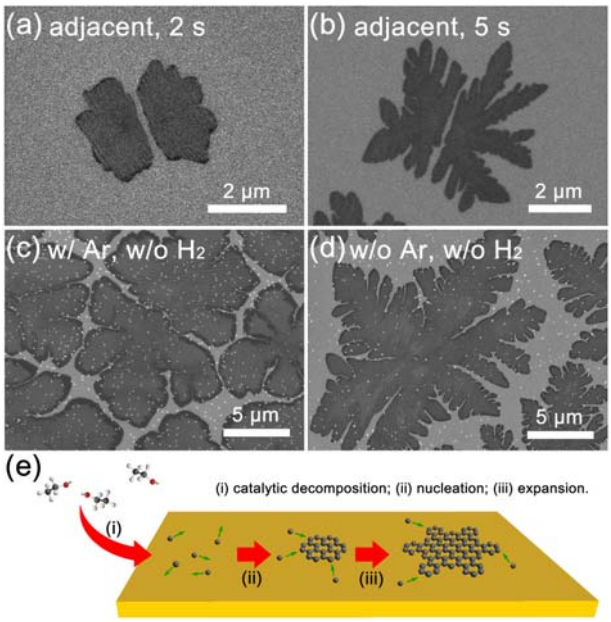

Figure 5. (a, b) SEM images of two adjacent graphene domains on copper after an ethanol exposure time of (a) 2 s and (b) 5 s. (c, d) SEM image of dendritic graphene domains grown on copper after 30 s exposure to ethanol (c) without hydrogen and (d) without any carrier gas. (e) Schematic of the initial state of the growth of graphene on copper from ethanol.

The above discussions are based on graphene grown by ethanol diluted with Ar/H_2 gas, and the effects from this dilution gas need to be addressed. Firstly we investigated the effect of hydrogen. In the case of methane, hydrogen appears to serve as both an activator of the surface-bound carbon and an etching reagent that controls the size and morphology of the graphene domains.[21,26] As for ethanol, trials using Ar instead of Ar/H_2 to dilute the ethanol show no significant difference in growing graphene domains, as shown in Figure 5c. This indicates that hydrogen plays a minor or insignificant role in the formation of graphene on copper when ethanol is used as the precursor. We admit the possibility that the flux ratio of hydrogen to ethanol adopted in our case (0.9:1, i.e. H_2/C 0.45:1) is not high enough to induce morphology changes to the graphene domains.[26,36] Furthermore, when no dilution gas is used with the ethanol

vapor, growth of graphene islands progresses faster, and more snowflake-like dendritic shapes (Figure 5d) are formed than the islands grown from ethanol with Ar/H_2 dilution (Figure 2d) or Ar dilution (Figure 5c).

The six-lobed dendritic shapes of graphene domains grown atop the Cu(111)-dominant surface indicate that the growth of graphene from ethanol at LPCVD conditions is a substrate-mediated process rather than a direct adsorption of carbon atoms from the gas phase. A schematic of the graphene growth on copper from ethanol at the initial stages is shown in Figure 5e. (i) At high temperature of 1000 ºC, ethanol decomposes into different products as carbon suppliers,[37] which are catalyzed into active carbon species by copper and chemically adsorbed on its surface. The exact $CH_{x<4}$ form of such active carbon species has not been well defined,[38,39] so we simply assume them as atomic carbon and describe as "carbon atoms" in the following discussion. Because the activation energy of surface diffusion of a carbon atom on copper is low (~0.06 eV),[40,41] at this high temperature carbon atoms almost freely diffuse and aggregate on the active sites of the copper surface to reach a critical supersaturation state[42] and start to nucleate in this supersaturated carbon field. (ii) The diffused carbon atoms on the copper surface are captured by the edge of the nuclei and form a circular shape due to initial "capillarity limitation", which reduces the interfacial free energy and decays the growth instabilities.[43,44] Jacobberger et al. have shown that the critical island size of such circular shape is 1 μm.[36] (iii) When the nucleated islands grow further, they are supplied with carbon atoms diffused from the copper surface rather than from the graphene surface because carbon surface density is lower on graphene due to less decomposition of carbon precursors on graphene. Therefore, a circular shape becomes unstable and morphological instabilities start to dominate the growth process.[45,46] There can be two origins for the dendritic shape: one is the anisotropy of growth rate depending

on the graphene crystal edge structure, and the other is the anisotropy of surface diffusion on the copper surface depending on the crystallographic orientation. In our result, apparently, anisotropic diffusion rates of carbon atoms along the crystallographic orientations determine the final dendritic shape of the graphene island, for instance, the six-lobed dendritic graphene domains on the six-fold Cu(111) surface. (iv) Because the active carbon atoms are only catalyzed on the copper surface, the narrow spacing in between places where two or more islands are adjacent severely limits the supply of active carbon atoms for surface diffusion, thus slowing the coalescence of these neighboring islands. After most of the graphene domains have coalesced, the lack of diffused active carbon atoms eliminates the growth of the secondary nucleated layer, resulting in the self-limiting growth of a continuous sheet of monolayer graphene.

The growth mechanism described above is analogous to what has been proposed for the self-limiting growth of graphene on copper from methane in LPCVD.[17,22,23,36,39] It shows that when the carbon flux is sufficiently low, the nucleation and expansion of graphene domains are independent of the precursor structures of ethanol and methane.

3.2. Comparison of graphene growth on different copper foils

To investigate the dependence of graphene growth on the underlying copper morphology in LPCVD, copper foils with differing facet distributions were used in identical CVD trials. In addition to the copper foil used in all experiments described above [electroplated side of YB-10, hereafter referred to as (111)-dominant Cu], we used different types of copper foils as described previously. For example, we show the domain growth of graphene on both the electroplated sides and drum sides for three different types of electroplated copper foils (10-μm-thick, product No. YB-10; 12-μm-thick, product No. Y-12; 9-μm-thick, product No. SLP-9; all provided by Nippon

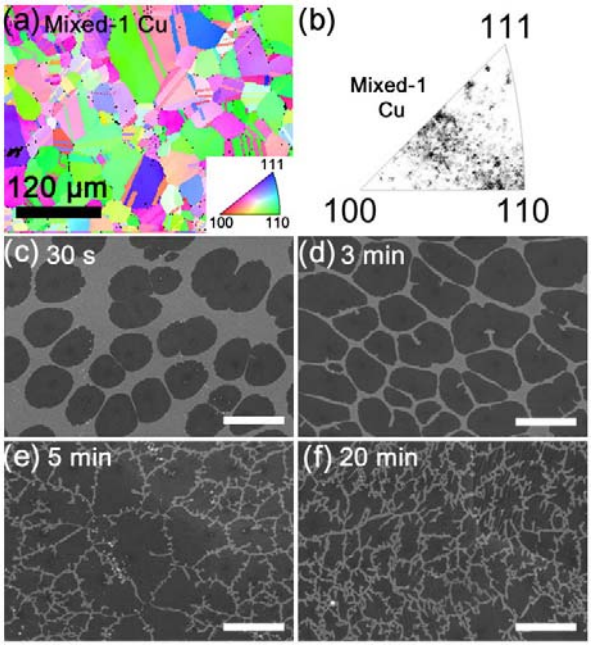

Figure 6. (a) EBSD mosaic map and (b) facet distribution of a Mixed-1 Cu foil. Black, red and yellow dots in (b) indicate high, medium and low facet probabilities, respectively. (c-f) Graphene morphology grown on the Mixed-1 Cu foil after (c) 30 s, (d) 3 min, (e) 5 min and (f) 20 min exposure to ethanol. No self-limiting growth can be obtained on this foil. Scale bars in (c-f): 5 μm.

Denkai, Ltd.) in Figure S7 in SI. All the resulting graphene domains are different in their shapes and nucleation locations, even on the electroplated sides of these copper foils.

We also focused on two other polycrystalline copper foils (10-μm-thick, product No. 113173, purchased from Nilaco Co., Ltd., referred as Mixed-1 Cu; drum side of YS-12, referred as Mixed-2 Cu) and a single-crystal copper foil (25-μm-thick, product No. 10950, purchased from Alfa Aesar Puratronic, referred as Single-crystal Cu). The EBSD map and facet distribution for Mixed-1 Cu are shown in Figures 6a and b. SEM images of various growth stages are shown in Figure 6c-f. The Mixed-1 Cu foil is crystallographically diverse with low-index Cu(110) facet and various high-index facets. These high-index facets are comprised of low-index facets with

different weights, meaning numerous atomic steps exist over the copper surface, as shown in the schematic of Figure S8 in SI. The domains grown on Mixed-1 Cu are circular in shape, suggesting no significant difference in the graphene growth rates for different orientations. This is because the facet dimensions are smaller than the surface diffusion length of carbon atoms on copper, altering the diffusion field in which the surface carbon flux is rather isotropic. These circular-shaped domains are different from all those previously reported with other shapes under similar growth conditions.[19-21,26,30,36,47,48] The SEM images also show it is easier for secondary nucleation to occur on the Mixed-1 Cu foils, and this secondary nucleation can expand over large areas with extended growth time (see Figure S9 in SI). More importantly, self-limiting growth of monolayer graphene cannot be obtained on Mixed-1 Cu foils, as shown in Figures 6e and f. Longer exposure time to ethanol results in more etching of existing graphene islands instead of the coalescence of adjacent islands. Furthermore, the layer number of graphene also increases when the growth time increases, because the unfilled gaps between adjacent domains can behave as diffusion channels for more carbon species, which are critical for the nucleation and expansion of new graphene layers.[49] Therefore, to form a continuous graphene sheet, a two-step growth is required,[22] i.e., growth at low-pressure for 3 min followed by high pressure for 15 s, but the resultant graphene contains numerous two-layer and few-layer flakes.

The EBSD map and facet distribution for Mixed-2 Cu are shown in Figure 7a and b, and the corresponding domains after growth of 30 s and 3 min are shown in Figure 7c and d, respectively. Although the Mixed-2 Cu foil is also crystallographically diverse, unlike Mixed-1 Cu the surface consists of more low-index facets of Cu(111) and Cu(100). The graphene domains after 30 s growth time show irregular shapes with rigid edges, significantly different from the circular shapes grown on the Mixed-1 Cu foils. A pronounced difference between these two

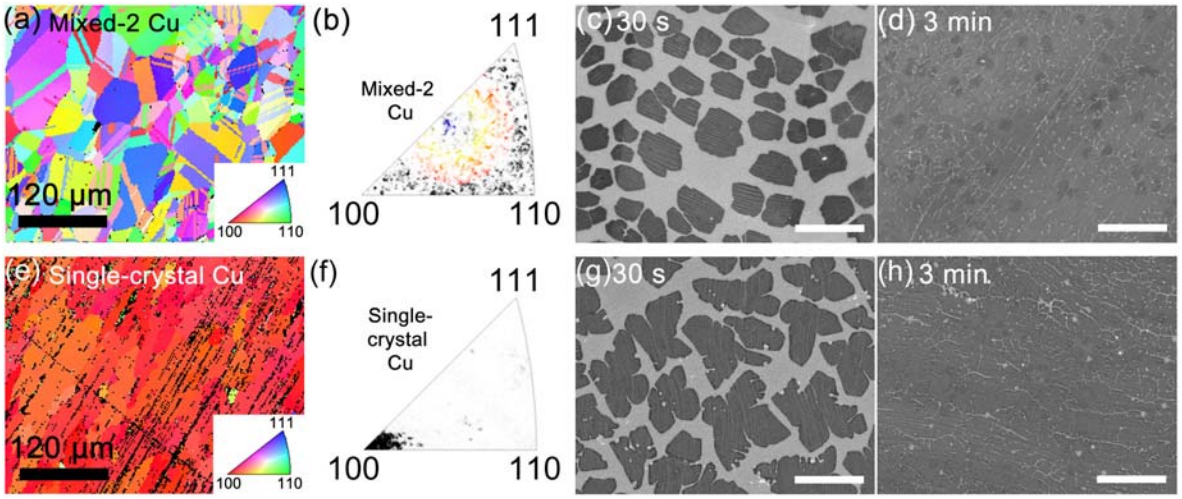

Figure 7. (a, e) EBSD mosaic maps of the (a) Mixed-2 Cu and (e) Single-crystal Cu copper foils. (b, f) Facet distributions derived from the EBSD maps for (b) Mixed-2 Cu and (f) Single-crystal Cu copper foils. Black, red and yellow dots indicate high, medium and low facet coverage, respectively. (c, d) Graphene morphology grown on the Mixed-2 Cu foil after (c) 30 s and (d) 3 min exposure to ethanol. (g, h) Graphene morphology grown on the single-crystal Cu foil after (g) 30 s and (h) 3 min exposure to ethanol. Scale bars in (c, d, g, h): 5 μm.

polycrystalline foils is the existence of the low-index facets of Cu(111) and Cu(100), whose lattice axes may play a key role in the formation of the rigid edges. The domains grown on Mixed-2 Cu coalesce with extend growth time, as shown in Figure 7d, but large flakes of secondary layers are also clearly visible (dark areas in Figure 7d). Considering that these large secondary flakes only occur on Mixed-1 Cu and Mixed-2 Cu foils, in which Cu(110) and high-index facets are dominant, the atomic arrangements on these copper surfaces are clearly a key factor for the secondary nucleation and formation of the new graphene layer. Self-limiting growth of a continuous graphene sheet can be obtained on Mixed-2 Cu foils, but with large flakes of secondary layers clearly seen.

To compare with the previous three types of polycrystalline copper foils, we conducted experiments using a single-crystal copper foil (Single-crystal Cu) with Cu(100) facet. Its EBSD maps and facet distribution are shown in Figures 7e and f, and the resulting graphene domains are shown in Figures 7g and h. The domains after 30 s ethanol exposure show four-lobed star-like shapes, consistent with the four lattice axes of the Cu(100) facet. This observation strengthens our previous conclusion that the graphene growth at LPCVD conditions is a substrate-mediated process. Coalescence of domains is also expected on these Single-crystal Cu foils, as shown in Figure 7h, and longer ethanol exposure time results in a self-limiting growth of monolayer graphene without apparent secondary nucleation spots.

This comparison of growth behaviors on the four different copper foils clearly shows that the self-limiting growth of monolayer graphene depends on the existence of different copper facets. The low-index facets of Cu(111) and Cu(100) provide diffusion channels for carbon adatoms to coalesce into domains, whereas the Cu(110) and high-index facets allow for nucleation and expansion of secondary layers. This means that the atomic arrangement of the underlying copper substrate is responsible for self-limiting growth of monolayer graphene in LPCVD condition. It needs to be noted that this facet-dependent growth behavior is different from that reported for the APCVD process, in which high-index copper facets do not act as barriers for the continuity of a graphene sheet.[27] An explanation for this is the higher pressure of precursor generates more active carbon atoms and reduces the effective diffusion length, hence, accelerates the nucleation at the copper steps of high-index facets, which results in more graphene nuclei to expand into a continuous graphene sheet.

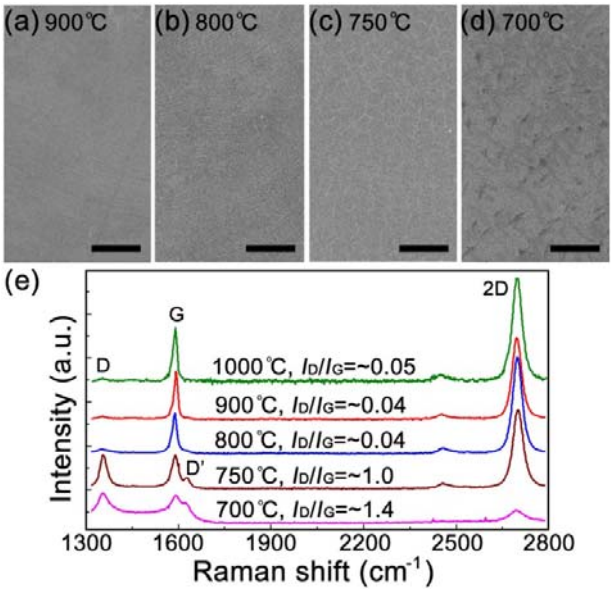

Figure 8. (a-d) SEM images of graphene grown on (111)-dominant Cu foils by 10 min exposure to ethanol at CVD temperatures of (a) 900 ºC, (b) 800 ºC, (c) 750 ºC, and (d) 700 ºC. All samples were annealed for 20 min at 1000 ºC prior to ethanol exposure. Scale bars: 5 μm. (e) Typical Raman spectra corresponding to graphene shown in (a-d).

Moreover, as shown in Figure 2d, Figure 6c and Figures 7c and g, graphene grown on Cu(111) has the highest growth rate compared with other facets, and growth on Cu(100) is slower than on the Cu(111) facet, but still faster than on copper facets with high indices.

3.3. Temperature window of graphene growth from ethanol

Finally we study the temperature window of graphene growth on copper from ethanol. After annealing under an Ar/H_2 mixture gas at 1000 ºC, the temperature was reduced. SEM images of graphene grown with lowered reaction temperature are shown in Figures 8a-d. All the graphene films grown at reduced temperature appear homogeneous, but careful observations of graphene films grown at 750 ºC and 700 ºC show some discontinuity with unfilled gaps. Corresponding Raman spectra in Figure 8e also indicate a significant decrease in the graphene quality, as highlighted by the increased D-band intensities. The Raman spectra of graphene grown at 900 ºC

and 800 ºC exhibit a low I_D/I_G of ~0.04, comparable with that for samples grown at 1000 ºC. However, when the growth temperature is further reduced to 750 ºC, the I_D/I_G value increases to ~1.0 and a D′-band appears, but the I_{2D}/I_G value remains at ~2. The increase of I_D/I_G may arise from the discontinuity of the graphene grown at 750 ºC. At 700 ºC, although sp^2-carbon-related Raman peaks of D, G and 2D-bands can be detected, features of monolayer graphene disappear, a large D′-band is present, and the corresponding I_D/I_G value further increases to ~1.4. The above results show that by using ethanol as a precursor, high quality, uniform, and continuous graphene films can be grown even when the reaction temperature is lowered to 800 ºC. In contrast, no continuous graphene films can be grown from methane at temperatures below 1000 ºC.[39] Moreover, the growth of high-quality graphene on copper substrate is highly dependent on the initial annealing temperature. Annealing the copper surface at 1000 ºC appears to be critical for obtaining high-quality graphene from ethanol at reduced growth temperature (see Figure S10 in SI). Low temperature annealing (e.g., at 800 ºC) introduces high D-bands in the corresponding Raman spectra of graphene, indicating poor-quality graphene films.

4. Conclusions

We systematically investigated self-limiting graphene growth on copper surfaces with facet distributions using ethanol as the carbon precursor. Using folded copper foil enclosures with crimped edges to sufficiently reduce the ethanol flux, the resulting graphene domains exhibit expansion behavior analogous to graphene grown from methane under low-pressure conditions. This indicates that when the carbon flux is sufficient low, nucleation and formation of graphene domains on the copper surface are independent of the precursor structures of ethanol and methane. Comparison of graphene growth on copper foils having differing facet distributions

show that graphene growth is a substrate-mediated process, and the shapes of the resulting graphene domains are determined by the symmetry of the underlying facet. Low-index copper facets of Cu(111) and Cu(100) play a crucial role in the coalescence of graphene domains and completion of the self-limiting process, whereas Cu(110) and high-index facets are critical for the nucleation and expansion of secondary graphene layers. Synthesis of graphene with I_D/I_G of ~0.04 from ethanol at only 800 ºC is also confirmed. Considering the high quality of graphene obtainable at lower reaction temperature, the demonstrated ability to produce self-limiting monolayer graphene, and no need for hydrogen addition makes ethanol a very attractive alternative to methane for CVD synthesis of high-quality graphene.

Supporting Information Available: Supplementary figures for the ACCVD system, more SEM images and Raman spectra. This material is available free of charge via the Internet at http://pubs.acs.org.

Acknowledgment. Part of this work was supported by Grants-in-Aid for Scientific Research (22226006, 23760179, and 23760180), and the Global COE Program "Global Center of Excellence for Mechanical Systems Innovation". Part of the characterization in this work was conducted at the Research Hub for Advanced Nano Characterization, The University of Tokyo, supported by the Ministry of Education, Culture, Sports, Science and Technology (MEXT), Japan. We acknowledge Mr. Shigeru Ohtsuka from the Institute of Engineering Innovation for the EBSD-SEM measurements, and the National Institute for Materials Science (NIMS) for scanning micro-Raman spectra. We also thank Nippon Denkai, Ltd. for supplying electroplated copper foil samples.

References

(1) Lee, C.; Wei, X. D.; Kysar, J. W.; Hone, J. *Science* **2008**, *321*, 385-388.

(2) Morozov, S. V.; Novoselov, K. S.; Katsnelson, M. I.; Schedin, F.; Elias, D. C.; Jaszczak, J. A.; Geim, A. K. *Phys. Rev. Lett.* **2008**, *100*, 016602.

(3) Liao, L.; Lin, Y. C.; Bao, M. Q.; Cheng, R.; Bai, J. W.; Liu, Y. A.; Qu, Y. Q.; Wang, K. L.; Huang, Y.; Duan, X. F. *Nature* **2010**, *467*, 305-308.

(4) Seol, J. H.; Jo, I.; Moore, A. L.; Lindsay, L.; Aitken, Z. H.; Pettes, M. T.; Li, X. S.; Yao, Z.; Huang, R.; Broido, D.; Mingo, N.; Ruoff, R. S.; Shi, L. *Science* **2010**, *328*, 213-216.

(5) Balandin, A. A. *Nat. Mater.* **2011**, *10*, 569-581.

(6) Novoselov, K. S.; Geim, A. K.; Morozov, S. V.; Jiang, D.; Zhang, Y.; Dubonos, S. V.; Grigorieva, I. V.; Firsov, A. A. *Science* **2004**, *306*, 666-669.

(7) Stankovich, S.; Dikin, D. A.; Piner, R. D.; Kohlhaas, K. A.; Kleinhammes, A.; Jia, Y.; Wu, Y.; Nguyen, S. T.; Ruoff, R. S. *Carbon* **2007**, *45*, 1558-1565.

(8) Berger, C.; Song, Z. M.; Li, X. B.; Wu, X. S.; Brown, N.; Naud, C.; Mayou, D.; Li, T. B.; Hass, J.; Marchenkov, A. N.; Conrad, E. H.; First, P. N.; de Heer, W. A. *Science* **2006**, *312*, 1191-1196.

(9) Sutter, P. W.; Flege, J. I.; Sutter, E. A. *Nat. Mater.* **2008**, *7*, 406-411.

(10) Reina, A.; Jia, X. T.; Ho, J.; Nezich, D.; Son, H. B.; Bulovic, V.; Dresselhaus, M. S.; Kong, J. *Nano Lett.* **2009**, *9*, 30-35.

(11) Kim, K. S.; Zhao, Y.; Jang, H.; Lee, S. Y.; Kim, J. M.; Kim, K. S.; Ahn, J. H.; Kim, P.; Choi, J. Y.; Hong, B. H. *Nature* **2009**, *457*, 706-710.

(12) Li, X. S.; Cai, W. W.; An, J. H.; Kim, S.; Nah, J.; Yang, D. X.; Piner, R.; Velamakanni, A.; Jung, I.; Tutuc, E.; Banerjee, S. K.; Colombo, L.; Ruoff, R. S. *Science* **2009**, *324*, 1312-1314.

(13) Gao, L. B.; Ren, W. C.; Xu, H. L.; Jin, L.; Wang, Z. X.; Ma, T.; Ma, L.-P.; Zhang, Z. Y.; Fu, Q.; Peng, L.-M.; Bao, X. H.; Cheng, H.-M. *Nat. Commun.* **2012**, *3*, 699.

(14) Lee, S.; Lee, K.; Zhong, Z. H. *Nano Lett.* **2010**, *10*, 4702-4707.

(15) Bae, S.; Kim, H.; Lee, Y.; Xu, X. F.; Park, J. S.; Zheng, Y.; Balakrishnan, J.; Lei, T.; Kim, H. R.; Song, Y. I.; Kim, Y. J.; Kim, K. S.; Ozyilmaz, B.; Ahn, J. H.; Hong, B. H.; Iijima, S. *Nat. Nanotechnol.* **2010**, *5*, 574-578.

(16) Li, X. S.; Cai, W. W.; Colombo, L.; Ruoff, R. S. *Nano Lett.* **2009**, *9*, 4268-4272.

(17) Bhaviripudi, S.; Jia, X. T.; Dresselhaus, M. S.; Kong, J. *Nano Lett.* **2010**, *10*, 4128-4133.

(18) Petrone, N.; Dean, C. R.; Meric, I.; van der Zande, A. M.; Huang, P. Y.; Wang, L.; Muller, D.; Shepard, K. L.; Hone, J. *Nano Lett.* **2012**, *12*, 2751-2756.

(19) Yan, Z.; Lin, J.; Peng, Z. W.; Sun, Z. Z.; Zhu, Y.; Li, L.; Xiang, C. S.; Samuel, E. L.; Kittrell, C.; Tour, J. M. *ACS Nano* **2012**, *6*, 9110-9117.

(20) Li, X. S.; Magnuson, C. W.; Venugopal, A.; Tromp, R. M.; Hannon, J. B.; Vogel, E. M.; Colombo, L.; Ruoff, R. S. *J. Am. Chem. Soc.* **2011**, *133*, 2816-2819.

(21) Zhang, Y.; Zhang, L. Y.; Kim, P.; Ge, M. Y.; Li, Z.; Zhou, C. W. *Nano Lett.* **2012**, *12*, 2810-2816.

(22) Li, X. S.; Magnuson, C. W.; Venugopal, A.; An, J. H.; Suk, J. W.; Han, B. Y.; Borysiak, M.; Cai, W. W.; Velamakanni, A.; Zhu, Y. W.; Fu, L. F.; Vogel, E. M.; Voelkl, E.; Colombo, L.; Ruoff, R. S. *Nano Lett.* **2010**, *10*, 4328-4334.

(23) Hwang, C.; Yoo, K.; Kim, S. J.; Seo, E. K.; Yu, H.; Biro, L. P. *J. Phys. Chem. C* **2011**, *115*, 22369-22374.

(24) Nie, S.; Wofford, J. M.; Bartelt, N. C.; Dubon, O. D.; McCarty, K. F. *Phys. Rev. B* **2011**, *84*, 155425.

(25) Robertson, A. W.; Warner, J. H. *Nano Lett.* **2011**, *11*, 1182-1189.

(26) Vlassiouk, I.; Regmi, M.; Fulvio, P. F.; Dai, S.; Datskos, P.; Eres, G.; Smirnov, S. *ACS Nano* **2011**, *5*, 6069-6076.

(27) Rasool, H. I.; Song, E. B.; Allen, M. J.; Wassei, J. K.; Kaner, R. B.; Wang, K. L.; Weiller, B. H.; Gimzewski, J. K. *Nano Lett.* **2011**, *11*, 251-256.

(28) Maruyama, S.; Kojima, R.; Miyauchi, Y.; Chiashi, S.; Kohno, M. *Chem. Phys. Lett.* **2002**, *360*, 229-234.

(29) Wassei, J. K.; Mecklenburg, M.; Torres, J. A.; Fowler, J. D.; Regan, B. C.; Kaner, R. B.; Weiller, B. H. *Small* **2012**, *8*, 1415-1422.

(30) Kidambi, P. R.; Ducati, C.; Dlubak, B.; Gardiner, D.; Weatherup, R. S.; Martin, M. B.; Seneor, P.; Coles, H.; Hofmann, S. *J. Phys. Chem. C* **2012**, *116*, 22492-22501.

(31) Dong, X. C.; Wang, P.; Fang, W. J.; Su, C. Y.; Chen, Y. H.; Li, L. J.; Huang, W.; Chen, P. *Carbon* **2011**, *49*, 3672-3678.

(32) Guermoune, A.; Chari, T.; Popescu, F.; Sabri, S. S.; Guillemette, J.; Skulason, H. S.; Szkopek, T.; Siaj, M. *Carbon* **2011**, *49*, 4204-4210.

(33) Chen, X.; Zhao, P.; Hou, B.; Einarsson, E.; Chiashi, S.; Maruyama, S. **2012**, submitted.

(34) Malard, L. M.; Pimenta, M. A.; Dresselhaus, G.; Dresselhaus, M. S. *Phys. Rep.* **2009**, *473*, 51-87.

(35) Nair, R. R.; Blake, P.; Grigorenko, A. N.; Novoselov, K. S.; Booth, T. J.; Stauber, T.; Peres, N. M. R.; Geim, A. K. *Science* **2008**, *320*, 1308-1308.

(36) Jacobberger, R. M.; Arnold, M. S. *Chem. Mater.* **2013**, *25*, 871-877.

(37) Xiang, R.; Hou, B.; Einarsson, E.; Zhao, P.; Harish, S.; Morimoto, K.; Miyauchi, Y.; Chiashi, S.; Tang, Z.; Maruyama, S. *ACS Nano* **2013**, 10.1021/nn305180g.

(38) Zhang, W. H.; Wu, P.; Li, Z. Y.; Yang, J. L. *J. Phys. Chem. C* **2011**, *115*, 17782-17787.

(39) Kim, H.; Mattevi, C.; Calvo, M. R.; Oberg, J. C.; Artiglia, L.; Agnoli, S.; Hirjibehedin, C. F.; Chhowalla, M.; Saiz, E. *ACS Nano* **2012**, *6*, 3614-3623.

(40) Yazyev, O. V.; Pasquarello, A. *Phys. Rev. Lett.* **2008**, *100*, 156102.

(41) Wu, P.; Zhang, W. H.; Li, Z. Y.; Yang, J. L.; Hou, J. G. *J. Chem. Phys.* **2010**, *133*, 071101.

(42) Luo, Z. T.; Kim, S.; Kawamoto, N.; Rappe, A. M.; Johnson, A. T. C. *ACS Nano* **2011**, *5*, 9154-9160.

(43) Mullins, W. W.; Sekerka, R. F. *J. Appl. Phys.* **1963**, *34*, 323-329.

(44) Sekerka, R. F. *J. Cryst. Growth* **1993**, *128*, 1-12.

(45) Saito, Y.; Uwaha, M. *Phys. Rev. B* **1994**, *49*, 10677-10692.

(46) Homma, Y.; Finnie, P.; Uwaha, M. *Surf. Sci.* **2001**, *492*, 125-136.

(47) Rasool, H. I.; Song, E. B.; Mecklenburg, M.; Regan, B. C.; Wang, K. L.; Weiller, B. H.; Gimzewski, J. K. *J. Am. Chem. Soc.* **2011**, *133*, 12536-12543.

(48) Zhang, B.; Lee, W. H.; Piner, R.; Kholmanov, I.; Wu, Y. P.; Li, H. F.; Ji, H. X.; Ruoff, R. S. *ACS Nano* **2012**, *6*, 2471-2476.

(49) Liu, L. X.; Zhou, H. L.; Cheng, R.; Yu, W. J.; Liu, Y.; Chen, Y.; Shaw, J.; Zhong, X.; Huang, Y.; Duan, X. F. *ACS Nano* **2012**, *6*, 8241-8249.

TOC Figure

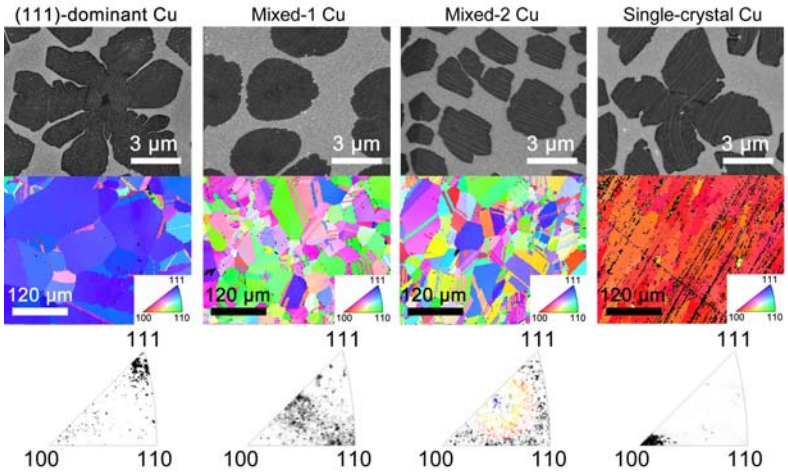
(111)-dominant Cu
Mixed-1 Cu
Mixed-2 Cu
Single-crystal Cu
3 μm
120 μm
111
100
110